Pergamon

Geochimica et Cosmochimica Acta, Vol. 63, No. 19/20, pp. 3153–3157, 1999

0016-7037/99 $20.00 + .00

PII S0016-7037(99)00242-2

X-ray standing wave study of arsenite incorporation at the calcite surface

LIKWAN CHENG[1,2] PAUL FENTER,[2] NEIL C. STURCHIO[2,*] ZHONG ZHONG,[3] and MICHAEL J. BEDZYK[1,4]

[1]Department of Materials Science and Engineering, and Materials Research Center, Northwestern University, Evanston, IL 60208 USA
[2]Environmental Research Division, Argonne National Laboratory, Argonne, IL 60439 USA
[3]National Synchrotron Light Source, Brookhaven National Laboratory, Upton, NY 11973 USA
[4]Materials Science Division, Argonne National Laboratory, Argonne, IL 60439 USA

(*Received October* 15, 1998; *accepted in revised form April* 29, 1999)

Abstract—The location and orientation of arsenite incorporated at the $CaCO_3$ $(10\bar{1}4)$ cleavage surface from a dilute aqueous solution was examined with the X-ray standing wave (XSW) technique. The high coherent fractions measured for As on the $(10\bar{1}4)$ and (0006) Bragg reflections indicate that the arsenite was well ordered in registration with the calcite surface lattice. The As coherent positions show that arsenite was located at the carbonate site. The XSW analysis is consistent with a structural model in which the pyramidal-shaped arsenite ion was oriented with its oxygen base coincident with the carbonate plane, and its As apex pointing outward from the $(10\bar{1}4)$ surface. The structure observed here for arsenite, and previously for selenite, suggests that other pyramidal trioxyanions could be incorporated at the calcite $(10\bar{1}4)$ surface with the same geometry. *Copyright © 1999 Elsevier Science Ltd*

1. INTRODUCTION

Trace molecular ion incorporation at ionic mineral surfaces can result from ion exchange, chemisorption, or coprecipitation at the mineral–fluid interface, and is relevant to many issues in the environmental and geologic sciences. The atomic scale structure of molecular ions incorporated as impurities at ionic crystal surfaces, however, is a relatively unexplored area in surface science (Masel, 1986). The scope of structural investigations for ionic impurities at surfaces has dealt mainly with monoatomic ions. A monoatomic ion can be described simply by its ionic radius and charge, whereas to describe the structure of a molecular ion requires consideration of the geometric and electronic configurations of its constituent atoms. Therefore, the structural compatibility between an ion and a surface site, known to be a key requirement for ion substitution, has a more subtle meaning in molecular ion substitution than in monoatomic ion substitution. How stringent is this site compatibility requirement for molecular ion substitution? If only molecular ions of an exactly identical configuration could substitute at a surface, the choice of suitable ions, and therefore, the probability of exchange, would be extremely restricted. In contrast, if molecular ions of roughly comparable size can substitute regardless of their detailed geometric configurations, the structural selectivity of surface incorporation would be minimized.

Studies of impurity incorporation during calcite growth have demonstrated conclusively that there is a significant selectivity depending not only on ionic size and charge, but also on the crystallographic direction in which crystal growth occurs (Paquette and Reeder, 1990; 1995; Staudt et al., 1994; Reeder, 1996). Surface sites can accommodate much larger fractions of impurity ions than bulk sites (e.g., Pb on calcite Sturchio et al., 1997). Although site geometry clearly exerts a dominant control on impurity ion incorporation, important questions remain regarding the range of impurity ions that may be incorporated at a given site, and the effect of variations in fluid composition and ion speciation (Hemming et al., 1995; Reeder, 1996).

A systematic approach toward answering these questions is to examine, for a given ionic surface, the incorporation of a series of impurity ions whose structures differ from those of the surface ions. Of the many structural classes of molecular ions, one of the simplest and most commonly occurring are the trioxyanions having the stoichiometric form BO_3, where B denotes the atom that binds to the oxygen atom covalently. This class of anions, along with the related BO_4 anions, represents the anionic portion of the salts of many common inorganic acids. The BO_3 anions have a trigonal symmetry, but are further divided into two groups: those whose B atoms have non-bonding valence shell electron pairs, which assume a pyramidal trigonal shape (including PO_3^{3-}, AsO_3^{3-}, SO_3^{2-}, SeO_3^{2-}, and BrO_3^-), and those whose B atoms do not have non-bonding valence shell electron pairs (including CO_3^{2-} and NO_3^-), which assume a planar trigonal shape.

The BO_3 anions are among the principal aqueous species of a number of environmentally and geochemically important elements (e.g., for B = C, N, Al, P, S, Cr, As, and Se). As a result, the interaction of such anions with mineral surfaces is significant in a wide range of geochemical cycles. Aqueous As and Se, for example, even in trace concentrations, are potential agents of human toxicity (National Research Council, 1983; Bagla and Kaiser, 1996). Recently, we reported an X-ray standing wave study of the structure of selenite incorporated at the calcite $(10\bar{1}4)$ surface (Cheng et al., 1997). Here we report an X-ray standing wave study of the structure of arsenite incorporated at this surface, and discuss the common structural features observed in both arsenite and selenite incorporation.

Arsenite incorporation at the calcite surface is important to the environmental behavior of arsenic. The As(III) and As(V) ions are the predominant naturally occurring inorganic forms of water-soluble As; As(III) species are more soluble and toxic than As(V) species (Cullen and Reimer, 1989). Chemical reactions involving As species at the mineral–water (and microorganism–water) interface play a critical role in determining

*Author to whom correspondence should be addressed (sturchio@anl.gov).

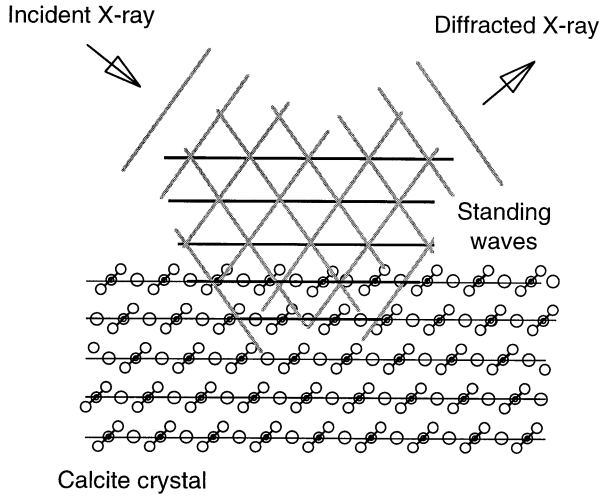

Fig. 1. Schematic diagram showing the XSW field generated by the Bragg diffraction from the calcite ($10\bar{1}4$) lattice planes. The diffraction plane spacing $d_{10\bar{1}4}$ is 3.04 Å. On the high-angle side of the Bragg-peak rocking curve, the *antinodal* planes of the XSW field are aligned with the ($10\bar{1}4$) diffraction planes, as shown. On the low-angle side of the rocking curve, the *nodal* planes are aligned with the ($10\bar{1}4$) diffraction planes. When the antinodes (nodes) of the XSW field are centered on fluorescent impurity atoms, the XSW field produces the maximum (minimum) fluorescence from these atoms. The measured fluorescence intensity versus the XSW location is used to locate the impurity atoms relative to the diffraction planes used to generate the XSW.

arsenic speciation, aqueous concentration, and human toxicity (Cullen and Reimer, 1989; Nriagu, 1994). Studies of As in natural waters have shown that As speciation is generally far from a state of thermodynamic equilibrium (Cherry et al., 1979; Aurilio et al., 1994). Recently, there have been a number of structural investigations of the interaction of As species at Fe-hydroxide surfaces (Waychunas et al., 1993; Manning et al., 1998; Sun and Doner, 1998). The incorporation of As species at the calcite surface, in spite of the ubiquity of calcite in the environment, has received much less attention.

2. EXPERIMENTAL METHODS

The Bragg-diffraction X-ray standing wave (XSW) technique used in this study is explained in a review (Zegenhagen, 1993). Briefly, from the dynamic theory of X-ray diffraction, it has been shown that an XSW field is generated from the coherent superposition of the incident and reflected X-ray beams during Bragg diffraction, and exists both within a perfect crystal and extends above its surface (Batterman and Cole, 1964; Batterman, 1969; Cowan et al., 1980). The wavelength of the XSW is equal to the lattice *d*-spacing of the diffraction planes. The XSW antinodes can be shifted relative to the diffraction planes by rocking the crystal in the X-ray incident angle θ through the arcsecond-wide Darwin curve of a Bragg reflection (see Fig. 1). By monitoring the modulation of the fluorescence yield from a specific atomic species versus the angle θ, one can determine the atomic position and distribution relative to the bulk diffraction plane. The fluorescence yield normalized with respect to that under non-Bragg condition varies as a function of the angle θ according to the following equation:

$$Y(\theta) = 1 + R(\theta) + 2\,[R(\theta)]^{1/2} f_H \cos[\nu(\theta) - 2\pi P_H]. \quad (1)$$

The reflectivity, $R(\theta)$, and the XSW phase, $\nu(\theta)$, are derived from dynamical diffraction theory. The coherent fraction, f_H, and the coherent position, P_H, for a selected $H = hkil$ diffraction plane of the substrate crystal lattice, represent the amplitude and phase of the H Fourier component of the spatial distribution of the atomic species. The coherent position, P_H, is the $\Delta d/d$ fractional position ranging from 0 to 1, where, for example, the value 0 and 1 correspond to the positions of adjacent diffraction planes, and 0.5 corresponds to a position halfway between the diffraction planes. The coherent fraction f_H, which also ranges from 0 to 1, measures the static and dynamic spread of the atomic distribution. The parameters f_H and P_H are obtained from a best χ^2-fit of Eqn. 1 to the XSW data after background subtraction. Uncertainties in f_H and P_H are typically smaller than ± 0.03, based on counting statistics and a sensitivity analysis of the fitting procedure.

The experimental procedure is based on that of a previous experiment in which selenite incorporation at the calcite surface was investigated (Cheng et al., 1997). The XSW measurements were made at the National Synchrotron Light Source (Upton, NY), at beamline X15A, and at the Advanced Photon Source (Argonne, IL), at beamline 12-ID-D. A dilute arsenous acid (H_3AsO_3) solution was reacted at room temperature with freshly cleaved ($10\bar{1}4$) surfaces of a natural calcite crystal. The As concentration in this solution was 51 μmol ($10^{-4.3}$ mol) and its pH was 9.81. The predominant As(III) species at pH 9.81 is $H_2AsO_3^-$ at thermodynamic equilibrium under moderately reducing conditions (Cullen and Reimer, 1989). The solution was exposed briefly to the atmosphere, thus some of the As may have become oxidized to As(V) species. However, because the exposure was brief and the kinetics of oxidation of As(III) species is slow (Cherry et al., 1979; van Elteren et al., 1991), it is likely that a large fraction of the As was present as As(III) species during the As(III) experiment. Also supporting the persistance of As(III) both in solution and as the adsorbed species is that identical experiments using a solution prepared with only As(V) species yielded no measurable incorporation of As at the calcite surface.

A total of six calcite surfaces were prepared and reacted by the following procedure, with comparable results. Adsorption was controlled by allowing the solution to react with the calcite surface for 8 to 10 min, after which the solution was swept from the calcite surface by a jet of dry nitrogen gas. The crystal was then placed in a He atmosphere for the duration of the XSW measurements. This procedure has been shown to be an effective way to examine impurities that are predominantly incorporated at the surface lattice sites, without generating a large excess of randomly precipitated species by evaporation of the solution (Cheng et al., 1997; Sturchio et al., 1997). The measurements were made using XSW generated from the ($10\bar{1}4$) and (0006) planes of the calcite. The calcite was precisely oriented in the X-ray beam by using a 4-circle diffractometer. The incident X-ray beam was collimated and monochromated with a Si(111) double-crystal monochromator at 12.9 keV. The Bragg reflectivity of the crystal and the As K_α fluorescence from the As were simultaneously recorded with a photodiode and a solid-state detector, respectively.

3. RESULTS AND DISCUSSION

The experimental results and best theoretical fits for reflectivity, $R(\theta)$, and As K_α fluorescence yield, $Y(\theta)$, with respect to the ($10\bar{1}4$) and the (0006) lattice planes are shown in Fig. 2. The corresponding values of coherent fractions and coherent positions extracted from the fits to Eqn. (1) are: $f_{10\bar{1}4} = 0.62 \pm 0.03$, $P_{10\bar{1}4} = 0.15 \pm 0.02$; and $f_{0006} = 0.50 \pm 0.10$, $P_{0006} = 0.27 \pm 0.06$. The average As surface coverage in the measured samples is 0.02 ± 0.01 monolayer (ML), as determined by comparing the As X-ray fluorescence intensity measurement of each sample against that of an As-implanted standard whose coverage had been determined by Rutherford backscattering spectroscopy (Chu et al., 1978). This coverage is significantly larger than that achievable through dense step edge incorporation alone; for surfaces having step densities typical of the calcite used in these experiments, the maximum coverage that could be incorporated at step edges is approximately 0.0006 ML (Sturchio et al., 1997).

The calcite ($10\bar{1}4$) surface has been shown by a number of

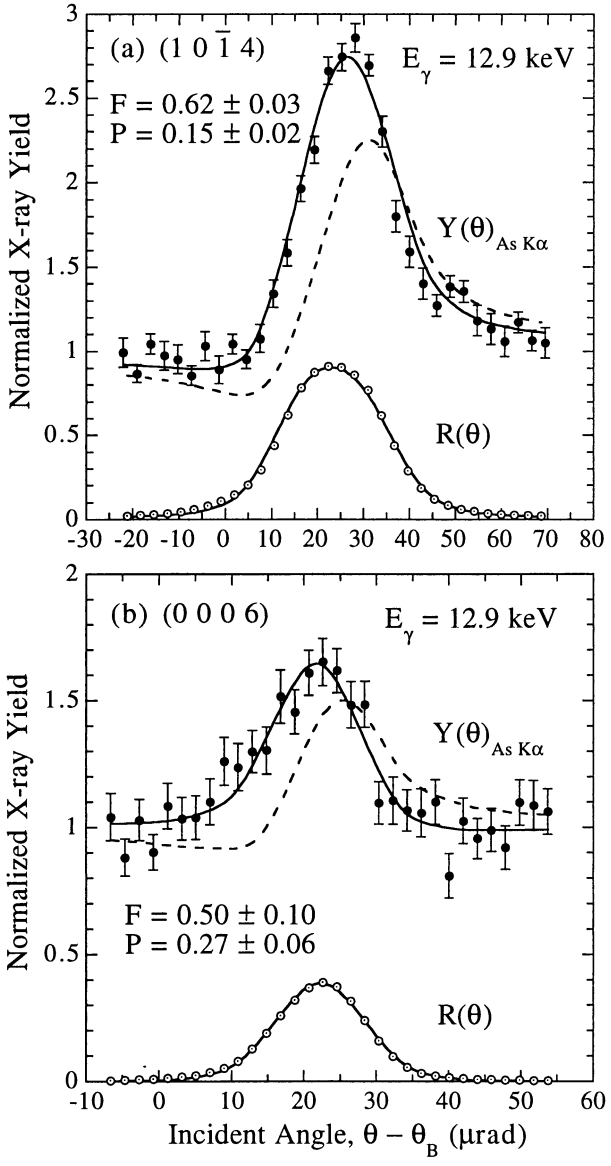

Fig. 2. The angular dependence of the experimental and theoretical X-ray reflectivity, $R(\theta)$ and As Kα fluorescence yield, $Y(\theta)$, for (a) the (10$\bar{1}$4) and (b) the (0006) Bragg reflections of calcite (solid curves). Also shown for comparison are the simulated fluorescence yield functions for the ideal C position at the measured As coherent fractions (dashed curves), calculated using Eqn. (1).

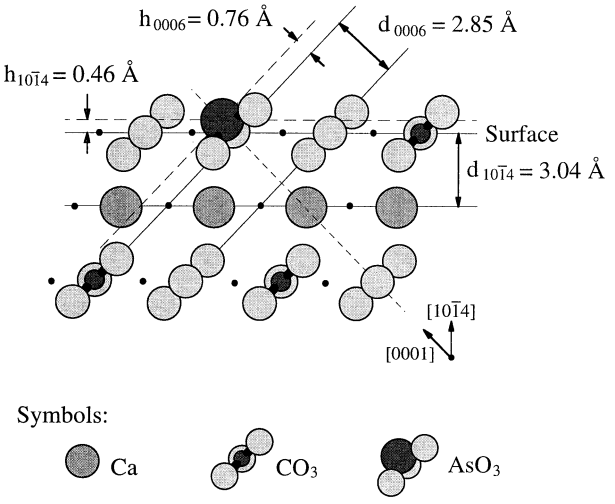

Fig. 3. Cross-sectional view of an ideally truncated calcite (10$\bar{1}$4) surface depicting the inferred atomic position of an arsenite ion substituting for a carbonate ion. Lattice points not in the cross section are indicated with small solid dots. The XSW-measured positions are indicated with dashed lines. The location of the As atom is given by the intersection of the dashed lines. The dotted line indicates the c-axis of the arsenite ion, in the [0001] direction of the lattice.

recent studies to be highly ordered in vacuo and in aquo. The in-plane surface unit cell has the bulk symmetry and cell parameter values of calcite (Stipp and Hochella, 1991; Ohnesorge and Binnig, 1993; Liang et al., 1996), although under certain conditions there can be significant vertical relaxations of Ca^{2+} and CO_3^{2-} ions at the calcite–water interface (de Leeuw and Parker, 1997; Fenter et al., 1998). The projected heights of the As atom in the [10$\bar{1}$4] and the [0006] directions, from the measured XSW coherent positions, are: $h_{10\bar{1}4}$ = 0.46 ± 0.06 Å and h_{0006} = 0.76 ± 0.17 Å, respectively, as calculated with the relation $h_H = P_H \times d_H$. In contrast, the bulk C atom (located at the origin of the unit cell) of the CO_3^{2-} group projects a height of zero length along any lattice normal; that is, $h_H = 0$ for any H. This comparison indicates a spatial displacement of the As position from the ideal C position. But this displacement is small compared to the distances from C to the Ca^{2+} ions surrounding the CO_3^{2-} molecule, and we conclude that the arsenite ion occupies the carbonate lattice site upon incorporation at the $CaCO_3$ (10$\bar{1}$4) surface.

The interpreted location of the As atom in the $CaCO_3$ (10$\bar{1}$4) surface lattice is shown in Fig. 3. The projected heights of the As position with respect to the (10$\bar{1}$4) and the (0006) lattice planes ($h_{10\bar{1}4}$ = 0.46 Å and h_{0006} = 0.76 Å) are indicated with dashed lines. The intersection of these dashed lines is the As position viewed in the plane containing the [10$\bar{1}$4] and the [0006] lattice vectors (the plane of the paper). Because the calcite (10$\bar{1}$4) surface unit cell has a two-fold symmetry in the direction normal to this plane, the average position of the As atom projected in the direction normal to this plane must be zero. That is, the average position of the As atoms must lie on the plane of the paper in Fig. 3, although the actual location of an individual As atom may be displaced normal to this plane.

In addition to the location of the As position, Fig. 3 also depicts a proposed orientation of the arsenite ion that is consistent with the XSW-measured As position. This structure takes into account the following symmetry factors in the arsenite and carbonate ions. First, there is a common three-fold rotational symmetry about the *c*-axis for both ions, and a reduced symmetry of the cyclic arsenite ion compared to the dihedral carbonate ion along the *c*-axis. Second, the Ca–O bond length is likely to be conserved, as in the case of cation incorporation (Cheng et al., 1998). A structure that agrees with these rationalizations is one in which the arsenite ion is oriented with its triangular oxygen base positioned in the carbonate oxygen plane. In the arsenite ion, the As–O distance is 1.84 Å and the O–As–O angle is 110° (Loewenschuss and Marcus, 1996). If the positions of the oxygen atoms in the arsenite ion are coincident with those of the carbonate ion, the projected

heights of the As atom in the [10$\bar{1}$4] and the [0006] directions are: ($h_{10\bar{1}4}$, h_{0006}) = (0.43, 0.60) Å, if the As apex is pointing in the +[0001] direction, or (2.61, 2.25) Å, if the As apex is pointing in the −[0001] direction. The position indicated by the first, and not the second, set of quantities agrees with the XSW results, where ($h_{10\bar{1}4}$, h_{0006}) = (0.46 ± 0.06, 0.76 ± 0.17) Å. Therefore, the inferred local structure of arsenite consistent with the experimental results has the As apex of the AsO_3 pyramid pointing upward (in the +[0001] direction), as shown in Fig. 3. One should not expect a perfect match between the model and the XSW-measured values, because the model does not take into account possible distortions in both the carbonate and arsenite ions at a surface site.

The As coherent positions from the XSW results only indicate that arsenite occupies the carbonate lattice site, but do not provide information on whether the arsenite is located above the (10$\bar{1}$4) surface, or incorporated in the surface monolayer or any subsurface layer. However, it seems unlikely that the arsenite ion is located above the calcite surface; assuming local carbonate bonding structure, it would have to be held to the surface layer by only one O–Ca bond. This structure would not be sufficiently stable to exhibit the high degree of ordering indicated by the high normal and off-normal As coherent fractions. Therefore, it is more likely that the arsenite ion is incorporated within the calcite lattice, either at or near the surface. From the functional form of $Y(\theta)$, we can demonstrate that the arsenite must be located within a small fraction of the 0.7 μm extinction depth from the surface.

The exact speciation of the arsenite, as incorporated within the calcite, cannot be determined from the XSW data. The dominant As(III) species in the initial solution at pH 9.81 is $H_2AsO_3^-$. Whether an accompanying deprotonation reaction may also occur, to result in the incorporation of a singly protonated divalent arsenite species ($HAsO_3^{2-}$) at the calcite surface is an interesting question. The local decrease in H^+ activity near the calcite surface as calcite dissolves in the initially undersaturated solution could cause deprotonation according to the equilibrium $H_2AsO_3^- + H^+ = HAsO_3^{2-}$. If the singly protonated species is incorporated, it would make sense that the single OH^- group of this species would protrude from the (10$\bar{1}$4) surface.

The As coherent positions for both the (10$\bar{1}$4) and (0006) planes agree well with those of Se in selenite incorporated at the calcite surface (i.e., $P_{10\bar{1}4} = 0.18$ and $P_{0006} = 0.22$; Cheng et al., 1997). The upward-pointing pyramid orientation agrees with the coherent positions observed in both arsenite- and selenite-incorporated (10$\bar{1}$4) surfaces. The similarity in their structure indicates that the mechanism of incorporation into calcite is similar for these ions.

The solutions that were reacted with calcite in these experiments were initially undersaturated with calcite, but would locally approach saturation with calcite as the surface dissolved. Calcite is the stable solid phase in the equilibrium system Ca-As(III)-CO_2-H_2O at 25°C, $pCO_2 = 10^{-3.5}$ atm, and $[As^{3+}] = 10^{-4.3}$ m (Nishimura et al., 1987). Therefore, arsenite could be incorporated into calcite by a dissolution–reprecipitation mechanism in a manner analogous to the formation of otavite–calcite solid solutions (Chiarello et al., 1997). The rates of calcite dissolution and precipitation under neutral to alkaline pH conditions, far from equilibrium, are on the order of 2 to 3 × 10^{-10} mol/cm^2/s (Plummer et al., 1979). At such rates, only several seconds would be required to dissolve or precipitate a monolayer of calcite (8.3 × 10^{-10} mol cm^{-2}); this is consistent with microscopic observations of step-edge velocities and typical step densities on calcite single crystals (MacInnis and Brantley, 1992; Gratz et al., 1993; Liang and Baer, 1997). Therefore, the maximum depth of As incorporation in an experiment where a relatively defect-free calcite crystal is reacted with the arsenite solution for 500 s would be in the range of 100 to 200 Å, if all of the calcite dissolved was then reprecipitated. The actual depth of As incorporation would generally be much less. An alternative mechanism for arsenite incorporation is through ion exchange reactions on flat terrace areas of the calcite surface, but this is more difficult to account for energetically, and in any case the dissolution–reprecipitation process also must occur because of the initial undersaturation of the solution with calcite.

The selective upward-pointing orientation of the pyramidal BO_3 ion, as a spatially isolated molecular point defect within the calcite (10$\bar{1}$4) surface lattice, must be justified by defect energy consideration. The difference in binding energy between the upward and downward pointing orientations is essentially electrostatic, and can be compared by considering their geometry, which is limited to an asymmetry in the [0001] direction. A comparison of the symmetry about the apical *B* atom for the upward and downward positions reveals that this energy difference is predominantly sensitive to the interactions between the *B* atom and the ions located along the [0001] axis (indicated with a short dashed line in Fig. 3). The upward-pointing orientation of the BO_3 ion is clearly the energetically favored of the two orientations, especially when the asymmetry induced by the surface is considered.

In summary, the local structure of arsenite incorporated at the calcite (10$\bar{1}$4) surface determined with X-ray standing wave technique shows that this ion is located at the carbonate position. The displacement of the As atom from the C site is in the +[0001] direction of the unrelaxed surface lattice.

Acknowledgments—This work was supported by the Geosciences Research Program, Office of Basic Energy Sciences, U.S. Department of Energy (DOE), under contract W-31-109-Eng-38 to Argonne National Laboratory (ANL). The National Synchrotron Light Source (NSLS) and the Advanced Photon Source (APS) are both supported by DOE. The NSLS beamline X15A is operated by ANL, Northwestern University and NSLS; the APS beamline 12ID-D is operated by the Basic Energy Sciences Synchrotron Radiation Center (ANL). We thank Rich Reeder, Susan Stipp, and two anonymous reviewers for constructive comments and suggestions.

REFERENCES

Aurilio A. C., Mason R. P., and Hemond H. F. (1994) Speciation and fate of arsenic in three lakes of the Aberjona watershed. *Environ. Sci. Tech.* **28,** 577–585.

Bagla P. and Kaiser J. (1996) Epidemiology: India's spreading health crisis draws global arsenic experts. *Science* **274,** 174–175.

Batterman B. W. (1969) Detection of foreign atoms by their X-ray fluorescence scattering. *Phys. Rev. Lett.* **22,** 703–705.

Batterman B. W. and Cole H. (1964) Dynamical diffraction of X-rays by perfect crystals. *Rev. Mod. Phys.* **36,** 681–717.

Cheng L., Lyman P., Sturchio N. C. and Bedzyk M. J. (1997) Adsorption and structure of selenite anions on the calcite (10$\bar{1}$4) surface. *Surf. Sci.* **382,** L690–L695.

Cheng L., Sturchio N. C., Woicik J., Kemner K., Lyman P. F., and

Bedzyk M. J. (1998) High resolution structural study of zinc ion incorporation at the calcite cleavage surface. *Surf. Sci.* **415,** 976–982.

Cherry J. A., Shaikh A. U., Tallman D. E., and Nicholson R. V. (1979) Arsenic species as an indicator of redox conditions in groundwater. *J. Hydrol.* **43,** 373–392.

Chiarello R. P., Sturchio N. C., Grace J., Geissbuhler P., Sorensen L., Cheng L., and Xu S. (1997). Otavite–calcite solid–solution formation at the calcite–water interface studied in situ by synchrotron X-ray scattering. *Geochim. Cosmochim. Acta* **61,** 1467–1474.

Chu W. K. , Mayer J. W., and Nicolet M.-A. (1978) *Backscattering Spectroscopy*. Academic Press.

Cowan P. L., Golovchenko J. A., and Robbins M. F. (1980) X-ray standing waves at crystal surfaces. *Phys. Rev. Lett*. **44,** 1680–1683.

Cullen W. R. and Reimer K. J. (1989) Arsenic speciation in the environment. *Chem. Rev.* **89,** 713–764.

De Leeuw N. H. and Parker S. C. (1997) Atomistic simulation of the effect of molecular adsorption of water on the surface structure and energies of calcite surfaces. *J. Chem. Soc. Faraday Trans.* **93,** 467–475.

Fenter P., Geissbühler P., DiMasi E., Srajer G., Sorensen L. and Sturchio N. (1998) Crystal truncation and water adsorption at the calcite-water interface. *Mineral. Mag.* **62A,** 1471–1472.

Gratz A. J., Hillner P. E., and Hansma P. K. (1993) Step dynamics and spiral growth on calcite. *Geochim. Cosmochim. Acta* **57,** 491–495.

Hemming N. G., Reeder R. J., and Hanson G. N. (1995) Mineral–fluid partitioning and isotopic fractionation of boron in synthetic calcium carbonate. *Geochim. Cosmochim. Acta* **59,** 371–379.

Liang Y. and Baer D. R. (1997) Anisotropic dissolution at the $CaCO_3$ $(10\bar{1}4)$ dissolution surface. *Surface Sci.* **373,** 275–287.

Liang Y., Lea A. S., Baer D. R., and Engelhard M. H. (1996) Structure of the cleaved $CaCO_3$ $(10\bar{1}4)$ surface in an aqueous environment. *Surf. Sci.* **351,** 172.

Loewenschuss A. and Marcus Y. (1996) Standard thermodynamic functions of gaseous polyatomic ions at 100–1000 K. *J. Phys. Chem. Ref. Data.* **25,** 1495.

MacInnis I. N. and Brantley S. L. (1992) The role of dislocations and surface morphology in calcite dissolution. *Geochim. Cosmochim. Acta* **56,** 1113–1126.

Manning B. A., Fendorf S. E., and Goldberg S. (1998) Surface structures and stability of arsenic(III) on goethite: Spectroscopic evidence for inner-sphere complexes. *Environ. Sci. Technol.* **32,** 2383–2388.

Masel R. I. (1986) *Principles of Adsorption and Reaction on Solid Surfaces.* Wiley.

National Research Council Subcommittee on Selenium (1983) *Selenium in Nutrition*. National Academy Press.

Nishimura T., Itoh C. T., and Tozawa K. (1987) Stabilities and solubilities of metal arsenites and arsenates in water and the effect of sulfate and carbonate ions on their solubilities. In *Arsenic Metallurgy Fundamentals and Applications* (ed.), pp. 77–89. The Metallurgical Society.

Nriagu J. O. (1994) *Arsenic in the Environment, Part I: Cycling and Characterization.* Wiley.

Ohnesorge F. and Binnig G. (1993) True atomic resolution by atomic force microscopy through attractive and repulsive forces. *Science* **260,** 1451–1456.

Paquette J. and Reeder R. J. (1990) New type of compositional zoning in calcite: Insights into crystal growth mechanisms. *Geology* **18,** 1244–1247.

Paquette J. and Reeder R. J. (1995) Relationship between surface structure, growth mechanism, and trace element incorporation into calcite. *Geochim. Cosmochim. Acta* **59,** 735–749.

Plummer L. N. , Parkhurst D. L., and Wigley T. M. L. (1979) Critical review of the kinetics of calcite dissolution and precipitation. In *Chemical Modeling of Aqueous Systems* (ed. E. A. Jenn), pp. 537–573. Amer. Chem. Soc. Symp. Series 93.

Reeder R. J. (1996) Interaction of divalent cobalt, zinc, cadmium, and barium with the calcite surface during layer growth. *Geochim. Cosmochim. Acta* **60,** 1543–1552.

Staudt W. J., Reeder R. J., and Schoonen M. A. A. (1994) Surface structural controls on compositional zoning of SO_4^{2-} and SeO_4^{2-} in synthetic calcite single crystals. *Geochim. Cosmochim. Acta* **58,** 2087–2098.

Stipp S. L. S. and Hochella M. F. Jr. (1991) Structure and bonding environments at the calcite surface as observed with X-ray photoelectron spectroscopy (XPS) and low energy electron diffraction. *Geochim. Cosmochim. Acta* **55,** 1723–1736.

Sturchio N. C., Chiarello R. P., Cheng L., Lyman P. F., Bedzyk M. J., Qian Y., You H., Yee D., Geissbuhler P., Sorenson L., Liang Y., and Baer D. (1997). Lead adsorption at the calcite-water interface: Synchrotron X-ray standing wave and X-ray reflectivity studies. *Geochim. Cosmochim. Acta* **61,** 251–264.

Sun X. and Doner H. E. (1998) Adsorption and oxidation of arsenite on goethite. *Soil Sci.* **163,** 278–287.

van Elteren J. T., Hoegee J., van der Hoek E. E., Das H. A., de Ligny C. L., and Agterdenbos J. (1991) Preservation of As(III) and As(V) in some water samples. *J. Radioanal. Nucl. Chem. Lett.* **154,** 343–355.

Waychunas G. A., Rea B. A., Fuller C. C., and Davis J. A. (1993) Surface chemistry of ferrihydrite: Part 1. EXAFS studies of the geometry of coprecipitated and adsorbed arsenate. *Geochim. Cosmochim. Acta* **57,** 2251–2269.

Zegenhagen J. (1993) Surface structure determination with X-ray standing waves. *Surf. Sci. Rep.* **18,** 199–271.